IEEE Open Journal of Signal Processing

Received 26 October 2022; revised 7 January 2023; accepted 7 January 2023. Date of publication 16 January 2023; date of current version 8 February 2023. The review of this article was arranged by Associate Editor Christos Masouros.

Digital Object Identifier 10.1109/OJSP.2023.3237040

Diversity Order Analysis for Quantized Constant Envelope Transmission

ZHEYU WU [1,2] (Graduate Student Member, IEEE), JIAGENG WU [3], WEI-KUN CHEN [4], AND YA-FENG LIU [1] (Senior Member, IEEE)

[1]LSEC, ICMSEC, AMSS, Chinese Academy of Sciences, Beijing 100190, China
[2]School of Mathematical Sciences, University of Chinese Academy of Sciences, Beijing 100049, China
[3]School of Mathematics, Jilin University, Changchun 130012, China
[4]School of Mathematics and Statistics, Beijing Institute of Technology, Beijing 100081, China

CORRESPONDING AUTHOR: YA-FENG LIU (e-mail: yafliu@lsec.cc.ac.cn).

The work of Zheyu Wu and Ya-Feng Liu was supported in part by the National Natural Science Foundation of China (NSFC) under Grants 12288201, 12022116, and 11991021. The work of Wei-Kun Chen was supported in part by the National Natural Science Foundation of China (NSFC) under Grant 12101048 and in part by the Beijing Institute of Technology Research Fund Program for Young Scholars.

ABSTRACT Quantized constant envelope (QCE) transmission is a popular and effective technique to reduce the hardware cost and improve the power efficiency of 5G and beyond systems equipped with large antenna arrays. It has been widely observed that the number of quantization levels has a substantial impact on the system performance. This paper aims to quantify the impact of the number of quantization levels on the system performance. Specifically, we consider a downlink single-user multiple-input-single-output (MISO) system with M-phase shift keying (PSK) constellation under the Rayleigh fading channel. We first derive a novel bound on the system symbol error probability (SEP). Based on the derived SEP bound, we characterize the achievable diversity order of the quantized matched filter (MF) precoding strategy. Our results show that full diversity order can be achieved when the number of quantization levels L is greater than the PSK constellation order M, i.e., $L > M$, only half diversity order is achievable when $L = M$, and the achievable diversity order is 0 when $L < M$. Simulation results verify our theoretical analysis.

INDEX TERMS Diversity order analysis, large antenna array, QCE transmission, SEP.

I. INTRODUCTION

Large antenna array is a promising technology to achieve high data rate and high reliability of wireless communication systems [1], [2], [3]. However, the power consumption and hardware cost of the system also grow with the number of antennas, which is a major concern for the practical implementation of the large antenna array technology. To address such issues, it is necessary to employ low-cost and energy-efficient hardware components at the base station (BS). It is well known that the most power hungry components at the BS are the power amplifiers (PAs) [4]. To improve the efficiency of the PAs, transmit signals with low peak-to-average power ratios (PAPRs) are desirable. In particular, constant envelope (CE) transmission, where the transmit signals from each antenna are restricted to have the same amplitude, has attracted a lot of research interests as it facilitates the use of the most efficient and cheapest PAs. It has been shown in the pioneering works [5], [6] that with N transmit antennas at the BS, an $O(N)$ array power gain is achievable for CE transmission, as in the case of conventional transmission schemes without the CE constraint. In addition, numerous well-designed CE transmission strategies have been proposed and have been shown (via simulations) to have good symbol error rate (SER) performance, see, e.g., [7], [8], [9], [10], [11] and the references therein. CE transmission has also found wide applications in many other scenarios [12], [13], [14].

However, a practical issue associated with CE transmission is that the digital-to-analog converters (DACs) at each antenna element must have infinite or very high resolution to ensure that the transmit signals can take any phase. This will lead to high hardware cost and power consumption of the communication system since high-resolution DACs are expensive and the power consumption of the DACs increases exponentially with the resolution number [15]. Due to this, a more

practical transmission scheme called quantized constant envelope (QCE) transmission [16] has been considered recently, where low-resolution DACs are employed and the phases of the transmit signals can only be selected from a (possibly small) finite set.

Existing works on QCE transmission mainly focused on precoding design [16], [17], [18], [19], [20], and in particular one-bit precoding design [21], [22], [23], [24], [25], [26], [27], [28], which is a special case of QCE transmission. The only few works that considered the performance analysis all focused on the one-bit case. Specifically, the authors in [21], [29] derived lower bounds on the achievable rate of a one-bit MIMO system. The result in [29] was further extended to the frequency selective channel in [30]. In [31], the authors considered the one-bit zero-forcing precoder and derived closed-form symbol error probability (SEP) approximations for large antenna array systems. To the best of our knowledge, there is still a theoretical gap in the performance analysis of general QCE transmission.

The motivation behind this work is based on the following observations that have been drawn from the simulations in existing works. First, the CE transmission can generally achieve good SER performance [6] while one-bit transmission sometimes suffers from a severe SER floor [21]. Second, slightly increasing the resolution of DACs from 1 bit to $2-3$ bits can sometimes significantly improve the SER performance of the system [20]. The goal of this paper is to theoretically characterize the system performance of a simple but popularly used QCE transmission strategy and shed some light on the above observations.

In this paper, we consider a downlink single-user MISO system with M-phase shift keying (PSK) modulation. The main contributions of this paper are twofold. First, we derive a new bound on the system SEP and the bound only involves an elegant quantity known as the safety margin [32], [33], [34]. The bound is universal and independently interesting, because it might be useful for the SEP analysis of possibly many communication scenarios. Second and more importantly, we characterize the diversity order of the quantized matched filter (MF) precoder. The reasons for the choice of the quantized MF precoder is that it is asymptotically optimal when the number of quantization levels goes to infinity in the considered system, and it admits a closed-form expression and thus is amenable to analysis. We show that the quantized MF precoder is able to achieve full diversity order when the number of quantization levels L is larger than M, while it can only achieve half and zero diversity order when $L=M$ and $L<M$, respectively. The above results hold as long as L and M are positive integers and $M>1$. Simulation results show that the analysis results are correct.

The remaining parts of this paper are organized as follows. Section II describes the system model and the problem formulation. Section III derives an important inequality on the SEP, which serves as the main tool for our analysis. Section IV gives the diversity order analysis. Simulation results are given in Section V to verify our theoretical results and the paper is concluded in Section VI.

Throughout the paper, we use x, $\boldsymbol{x}$, and $\mathcal{X}$ to denote scalar, vector, and set, respectively. For a scalar $x\in\mathbb{C}$, $|x|$, $\arg(x)$, $\mathcal{R}(x)$, and $\mathcal{I}(x)$ return the absolute value, the argument, the real part, and the imaginary part of x, respectively. For a vector $\boldsymbol{x}\in\mathbb{C}^n$, x_i denotes the i-th entry of $\boldsymbol{x}$ and $\|\boldsymbol{x}\|_p$ denotes the p-norm of $\boldsymbol{x}$, where $p\in\{1,2\}$; $\boldsymbol{x}^{\mathsf{T}}$, $\boldsymbol{x}^{\dagger}$, and $\boldsymbol{x}^{\mathsf{H}}$ denote the transpose, the conjugate, and the Hermitian transpose of $\boldsymbol{x}$, respectively. For a random variable X, we use $p_X(\cdot)$ and $F_X(\cdot)$ to denote its probability density function (PDF) and cumulative distribution function (CDF), respectively. $\mathbb{E}[\cdot]$ and $\mathbb{P}(\cdot)$ return the expectation and the probability of their corresponding argument, respectively. $\mathcal{CN}(0,\sigma^2)$ and $\mathcal{N}(0,\sigma^2)$ represent the zero-mean circularly symmetric complex Gaussian distribution and zero-mean Gaussian distribution (in the real space) with variance σ^2, respectively. Finally, j denotes the imaginary unit (satisfying $j^2=-1$).

II. SYSTEM MODEL AND PROBLEM FORMULATION

Consider a MISO system where an N-antenna BS serves a single-antenna user. Let $\mathbf{h}=(h_1,h_2,\ldots,h_N)^{\mathsf{T}}$ denote the channel vector between the BS and the user and $\boldsymbol{x}=(x_1,x_2,\ldots,x_N)^{\mathsf{T}}$ denote the transmitted signal from the BS. The signal received by the user can then be expressed as

$$y=\mathbf{h}^{\mathsf{T}}\boldsymbol{x}+n,$$

where $n\sim\mathcal{CN}(0,\sigma^2)$ is the additive white Gaussian noise. We assume that the entries of $\mathbf{h}$ are independent and identically distributed (i.i.d.) following $\mathcal{CN}(0,1)$.

In this paper, we consider QCE transmission, i.e., each antenna is only allowed to transmit QCE signals. Mathematically, the QCE constraint can be expressed as

$$x_i\in\mathcal{X}_L\triangleq\left\{\sqrt{\frac{P_T}{N}}e^{j\frac{(2l-1)\pi}{L}},l=1,2,\ldots,L\right\},i=1,2,\ldots,N,$$

where P_T is the total transmit power at the BS and L is the number of quantization levels, i.e., the number of points in $\mathcal{X}_L$. In what follows, we set $P_T=1$ for simplicity. Let s be the intended symbol for the user, which is independent of $\mathbf{h}$ and n. We focus on M-PSK constellation, i.e., s is uniformly drawn from $\mathcal{S}_M=\{e^{j\frac{2\pi(m-1)}{M}},m=1,2,\ldots,M\}$. We note here that in practice, both L and M should be a power of 2, and an L-level quantization corresponds to $(\log_2 L-1)$-bit quantization of DACs. However, since our analysis holds for arbitrary quantization level L and constellation order $M>1$, we choose to present our analysis and results in the most general form and just assume that L and M are positive integers and $M>1$ in the following.

In this paper, we adopt a simple QCE transmission strategy called quantized MF precoding:

$$\boldsymbol{x}=q_L(s\mathbf{h}^{\dagger}),\tag{1}$$

where $q_L(\cdot)$ is the quantization function that maps its argument component-wise to the nearest points in $\mathcal{X}_L$. The reasons for the choice of the quantized MF precoder are as follows. First, it is asymptotically optimal when the number of quantization levels L goes to infinity. More specifically, when there is no quantization (i.e., $L = \infty$), the transmitted signals of quantized MF precoding can be expressed as

$$x_i = \frac{1}{\sqrt{N}} e^{-j \arg(h_i)} s,\ i = 1, 2, \ldots, N, \tag{2}$$

with which the useful signal power is maximized. Second, the quantized MF precoder admits a closed-form expression (i.e., (1)) and is of low computational complexity, which is more practical and more amenable to analysis than many other transmission strategies depending on numerical solutions of certain discrete optimization problems (e.g., those in [17], [18], [19], [20]). With quantized MF precoding, the system model can be expressed as

$$y = \mathbf{h}^{\mathsf{T}} q_L(s\mathbf{h}^{\dagger}) + n = \frac{1}{\sqrt{N}} \sum_{i=1}^{N} |h_i| e^{j\theta_i} s + n, \tag{3}$$

where $\theta_i \in [-\frac{\pi}{L}, \frac{\pi}{L}]$, $i = 1, 2, \ldots, N$, are the quantization error (of angle). At the receiver side, we assume that nearest neighbor decoding is employed, that is, the user maps its received signal y to the nearest constellation point $\hat{s} \in \mathcal{S}_M$.

Our goal in this paper is to characterize the impact of the number of quantization levels on the system performance. We adopt the diversity order [35] as our performance metric[1], which is a classical metric that characterizes the rate at which the SEP, i.e., $\mathbb{P}(\hat{s} \neq s)$, tends to zero as the signal-to-noise-ratio (SNR) grows. Its definition is given by

$$d = \lim_{\rho \to +\infty} -\frac{\log \mathbb{P}(\hat{s} \neq s)}{\log \rho}, \tag{4}$$

where $\rho = \frac{1}{\sigma^2}$ is the SNR. Roughly speaking, the above definition says that in the high SNR regime, the SEP will scale as ρ^{-d}.

III. A NEW BOUND ON THE SEP

In this section, we derive a new bound on the system SEP. The new bound will serve as the main tool for our subsequent analysis and is independently interesting, because it might also be useful for the SEP analysis of other communication scenarios.

Consider the following system model:

$$y = \beta s + n, \tag{5}$$

where s is uniformly drawn from M-PSK constellation, $n \sim \mathcal{CN}(0, \sigma^2)$, and $\beta \in \mathbb{C}$ is a constant. Define

$$\alpha = \mathcal{R}(\beta) - |\mathcal{I}(\beta)| \cot \frac{\pi}{M}. \tag{6}$$

[1]There are also many other important performance metrics, including the spectral and energy efficiency. Investigating the impact of the number of quantization levels under these performance metrics can be interesting future works.

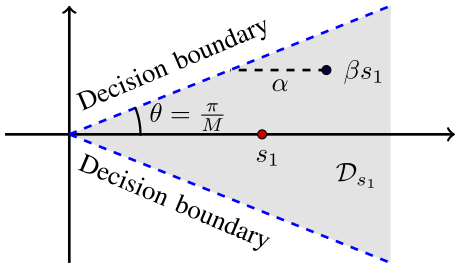

FIGURE 1. An illustration of the decision region $\mathcal{D}_{s_1}$ of symbol s_1 and its safety margin α.

The above quantity is well-known as the safety margin in the literature and is widely adopted as a performance metric for precoding design [32], [33], [34]. Geometrically, it characterizes the distance between the noise-free received signal and the decision boundary of the intended symbol, as shown in Fig. 1. It is widely believed that the safety margin has an essential impact on the system SEP. In the following theorem, we give a quantitative characterization of the relationship between the SEP and the safety margin α.

Theorem 1: The SEP of model (5) can be bounded as

$$Q\left(\frac{\sqrt{2}\sin\frac{\pi}{M}\alpha}{\sigma}\right) \leq \text{SEP} \leq 2Q\left(\frac{\sqrt{2}\sin\frac{\pi}{M}\alpha}{\sigma}\right), \tag{7}$$

where α is given in (6) and $Q(x) = \frac{1}{\sqrt{2\pi}} \int_x^{\infty} e^{-\frac{1}{2}x^2} dx$ is the tail distribution function of the standard Gaussian distribution.

Proof: Let $\mathcal{D}_s$ denote the decision region of symbol s and let $s_1, s_2, \ldots, s_M$ be the constellation points in $\mathcal{S}_M$, where $s_m = e^{\frac{j2\pi(m-1)}{M}}$. Then, the SEP can be expressed as

$$\text{SEP} = \mathbb{P}\left(y \notin \mathcal{D}_s\right) = \frac{1}{M} \sum_{m=1}^{M} \mathbb{P}\left(y \notin \mathcal{D}_s \mid s = s_m\right), \tag{8}$$

where the second equality holds since s is uniformly drawn from $\mathcal{S}_M$. Due to the symmetry of the PSK constellation, each probability in the above summation is equal and thus we only need to consider one of them. For simplicity, we consider $\mathbb{P}(y \notin \mathcal{D}_s \mid s = s_1)$, where $s_1 = 1$. Since nearest neighbor decoding is employed, the decision region of s_1 is

$$\begin{aligned}\mathcal{D}_{s_1} &= \left\{y \mid \arg(y) \in \left(-\frac{\pi}{M}, \frac{\pi}{M}\right)\right\} \\ &= \left\{y \mid |\mathcal{I}(y)| < \tan\frac{\pi}{M}\mathcal{R}(y)\right\};\end{aligned}$$

see Fig. 1 for an illustration of the decision region of s_1. Based on this, we can express $\mathbb{P}(y \notin D_s \mid s = s_1)$ as

$$\begin{aligned}\mathbb{P}(y \notin \mathcal{D}_s \mid s = s_1) &= \mathbb{P}(\beta + n \notin \mathcal{D}_{s_1}) \\ &= \mathbb{P}\left(|\mathcal{I}(\beta + n)| \geq \tan\frac{\pi}{M}\mathcal{R}(\beta + n)\right),\end{aligned}$$

which can further be lower and upper bounded by

$$\begin{aligned}
&\max\left\{\mathbb{P}\left(\mathcal{I}(\beta+n)\geq\tan\frac{\pi}{M}\mathcal{R}(\beta+n)\right),\right.\\
&\qquad\left.\mathbb{P}\left(\mathcal{I}(\beta+n)\leq-\tan\frac{\pi}{M}\mathcal{R}(\beta+n)\right)\right\}\\
&\leq\mathbb{P}\left(|\mathcal{I}(\beta+n)|\geq\tan\frac{\pi}{M}\mathcal{R}(\beta+n)\right)\\
&\leq\mathbb{P}\left(\mathcal{I}(\beta+n)\geq\tan\frac{\pi}{M}\mathcal{R}(\beta+n)\right)\\
&\quad+\mathbb{P}\left(\mathcal{I}(\beta+n)\leq-\tan\frac{\pi}{M}\mathcal{R}(\beta+n)\right).
\end{aligned}\tag{9}$$

For $\mathbb{P}(\mathcal{I}(\beta+n)\geq\tan\frac{\pi}{M}\mathcal{R}(\beta+n))$, we have

$$\begin{aligned}
&\mathbb{P}\left(\mathcal{I}(\beta+n)\geq\tan\frac{\pi}{M}\mathcal{R}(\beta+n)\right)\\
&=\mathbb{P}\left(\cot\frac{\pi}{M}\mathcal{I}(n)-\mathcal{R}(n)\geq\mathcal{R}(\beta)-\cot\frac{\pi}{M}\mathcal{I}(\beta)\right)\\
&=Q\left(\frac{\sqrt{2}\sin\frac{\pi}{M}}{\sigma}\left(\mathcal{R}(\beta)-\cot\frac{\pi}{M}\mathcal{I}(\beta)\right)\right),
\end{aligned}\tag{10}$$

where the last equality holds since $n\sim\mathcal{CN}(0,\sigma^2)$ and thus $\cot\frac{\pi}{M}\mathcal{I}(n)-\mathcal{R}(n)\sim\mathcal{N}(0,\frac{\sigma^2}{2\sin^2\frac{\pi}{M}})$. Similarly, we can show that

$$\begin{aligned}
&\mathbb{P}\left(\mathcal{I}(\beta+n)\leq-\tan\frac{\pi}{M}\mathcal{R}(\beta+n)\right)\\
&=Q\left(\frac{\sqrt{2}\sin\frac{\pi}{M}}{\sigma}\left(\mathcal{R}(\beta)+\cot\frac{\pi}{M}\mathcal{I}(\beta)\right)\right).
\end{aligned}\tag{11}$$

Note that $\alpha=\min\{\mathcal{R}(\beta)-\cot\frac{\pi}{M}\mathcal{I}(\beta),\mathcal{R}(\beta)+\cot\frac{\pi}{M}\mathcal{I}(\beta)\}$ and $Q(\cdot)$ is a decreasing function. Combining this with (8)–(11), we have the desired result in (7), which completes the proof. ■

Several remarks on Theorem 1 are in order. First, the upper bound in (7) has already been derived in [36]. Our proof is different from that in [36] and can give both lower and upper bounds in (7) simultaneously. It turns out that both the lower and upper bounds in (7) are important in the following diversity order analysis. Second, if β in (5) is a positive constant, i.e., $\beta>0$, then $\alpha=\beta$ and inequality (7) reduces to the following well-known inequality [37]:

$$Q\left(\frac{\sqrt{2}\sin\frac{\pi}{M}\beta}{\sigma}\right)\leq\text{SEP}\leq 2Q\left(\frac{\sqrt{2}\sin\frac{\pi}{M}\beta}{\sigma}\right).$$

Finally, Theorem 1 enables to characterize the SEP of the considered model (3), as shown in the following corollary.

Corollary 1: The SEP of model (3) can be bounded as

$$\mathbb{E}_\alpha\left[Q\left(\frac{\sqrt{2}\sin\frac{\pi}{M}\alpha}{\sigma}\right)\right]\leq\text{SEP}\leq 2\mathbb{E}_\alpha\left[Q\left(\frac{\sqrt{2}\sin\frac{\pi}{M}\alpha}{\sigma}\right)\right],\tag{12}$$

where

$$\alpha=\frac{1}{\sqrt{N}}\sum_{i=1}^{N}|h_i|\left(\cos\theta_i-|\sin\theta_i|\cot\frac{\pi}{M}\right).\tag{13}$$

Proof: The considered model (3) is in the form of (5) with

$$\beta=\frac{1}{\sqrt{N}}\sum_{i=1}^{N}|h_i|e^{j\theta_i}.\tag{14}$$

Note that β in (14) is a random variable, which is a function of both $\mathbf{h}$ and θ_i, $i=1,2,\ldots,N$. Applying the total probability theorem, we can express the SEP of model (3) as

$$\begin{aligned}
\text{SEP}=\mathbb{P}(\hat{s}\neq s)&=\int_{\beta\in\mathbb{C}}\mathbb{P}\left(\hat{s}\neq s\mid\beta=x\right)p_\beta(x)dx\\
&=\mathbb{E}_\beta\left(\mathbb{P}(\hat{s}\neq s\mid\beta)\right).
\end{aligned}\tag{15}$$

One can show that β and s are independent. Then it follows from (15) and Theorem 1 that

$$\mathbb{E}_\alpha\left[Q\left(\frac{\sqrt{2}\sin\frac{\pi}{M}\alpha}{\sigma}\right)\right]\leq\text{SEP}\leq 2\mathbb{E}_\alpha\left[Q\left(\frac{\sqrt{2}\sin\frac{\pi}{M}\alpha}{\sigma}\right)\right],$$

where α is given in (13). ■

In the following section, we will use Corollary 1 as the main tool to analyze the diversity order of the considered system.

IV. DIVERSITY ORDER ANALYSIS

In this section, we will first present our main diversity order results and give some explanations and discussions in Section IV-A and then give a detailed proof in Section IV-B.

A. MAIN RESULTS

We first summarize the diversity order results in the following theorem.

Theorem 2: For a single-user MISO system with N transmit antennas and M-PSK modulation, the achievable diversity order of the L-level quantized MF precoder in (1) is given by

$$d=\begin{cases}N, & \text{if } L>M;\\ \frac{N}{2}, & \text{if } L=M;\\ 0, & \text{if } L<M.\end{cases}$$

Theorem 2 clearly shows that the number of quantization levels has a vital impact on the achievable diversity order of the considered system. In particular, when the number of quantization levels L is greater than the PSK constellation order M, the system SEP will decrease quickly to zero as the SNR goes to infinity; on the other hand, when $L<M$, there will be a SEP floor, i.e., the system SEP will not decrease to zero even when the SNR tends to infinity. The interesting case is $L=M$ where the SEP of the system will decrease to zero as the SNR tends to infinity but with a slower rate compared to the case where $L>M$. We also mention here a related work [38], which gave diversity order analysis for an uplink single-input-single-output (SISO) system with low-resolution analog-to-digital converters (ADCs). Interestingly, the diversity order results in [38] are consistent with our results in Theorem 2 for $N=1$, though they are derived for different systems and communication scenarios using completely different analysis tools.

In the rest part of this subsection, we will give an intuitive explanation of the diversity order results in Theorem 2. The discussions below are somewhat heuristic but shed useful light on why different diversity order results are obtained for the three different cases in Theorem 2. A rigorous proof of Theorem 2 will be provided in the next subsection.

To begin, we give some intuitions on the relationship between the safety margin α in (6) and the system SEP. It is obvious that in the noiseless case (i.e., $\rho = \infty$), the intended symbol will be incorrectly decoded if and only if $\alpha \leq 0$, which corresponds to the case where the noiseless received signal lies outside the decision region of the intended symbol (see Fig. 1), i.e., SEP $= \mathbb{P}(\alpha \leq 0)$. In the general case, roughly speaking, the safety margin describes how large the order of magnitude the additive noise is allowed to have such that the received signal still lies within the decision region, in which case an error will not occur. Note that as ρ tends to infinity, the magnitude of the noise, i.e., $|n|$, is in the order of $\rho^{-\frac{1}{2}}$. Then, the above discussions imply that the SEP is in the same order as $\mathbb{P}(\alpha \leq \rho^{-\frac{1}{2}})$. Therefore, characterizing the diversity order is equivalent to studying how fast the probability $\mathbb{P}(\alpha \leq \rho^{-\frac{1}{2}})$ decreases as ρ tends to infinity, i.e.,

$$d = -\lim_{\rho \to +\infty} \frac{\log \mathbb{P}(\alpha \leq \rho^{-\frac{1}{2}})}{\log \rho}.$$

The above equality will be implicitly shown in the proof of Theorem 2 in the next subsection.

Next we focus on the estimation of $\mathbb{P}(\alpha \leq \rho^{-\frac{1}{2}})$. For the considered model, α in (13) is a sum of N i.i.d. random variables. We express α as $\alpha = \frac{1}{\sqrt{N}} \sum_{i=1}^{N} \alpha_i$, where

$$\alpha_i = |h_i| v_i \text{ and } v_i = \cos\theta_i - |\sin\theta_i| \cot\frac{\pi}{M} \tag{16}$$

with $h_i \sim \mathcal{CN}(0, 1)$ and θ_i uniformly distributed in $[-\frac{\pi}{L}, \frac{\pi}{L}]$. Note that when $L \geq M$, each α_i in (16) is nonnegative, and hence $\mathbb{P}(\alpha \leq \rho^{-\frac{1}{2}})$ is in the same order as $[\mathbb{P}(\alpha_i \leq \rho^{-\frac{1}{2}})]^N$ (see (25) and (30) further ahead for the rigorous expressions) and

$$d = -N \lim_{\rho \to +\infty} \frac{\log \mathbb{P}(\alpha_i \leq \rho^{-\frac{1}{2}})}{\log \rho}. \tag{17}$$

We next investigate the three cases in Theorem 2, i.e., $L > M$, $L = M$, and $L < M$, separately.

Case 1. $L > M$: In this case, v_i in (16) is bounded from below by a positive constant independent of ρ and thus has no effect on estimating $\mathbb{P}(\alpha_i \leq \rho^{-\frac{1}{2}})$ when ρ tends to infinity. As such, the distribution of $|h_i|$ will dominate in estimating $\mathbb{P}(\alpha_i \leq \rho^{-\frac{1}{2}})$, whose CDF is in the order of $O(x^2)$ when x is near 0, making $\mathbb{P}(\alpha_i \leq \rho^{-\frac{1}{2}})$ in the order of ρ^{-1}. Then, from (17), we have $d = N$.

Case 2. $L = M$: In this case, $v_i \geq 0$ and the probability of v_i being very close to 0 is nonzero. Consequently, either a small v_i or a small $|h_i|$ can result in a small α_i, in which case the CDF of α_i becomes in the order of $O(x)$ when x is near 0, and thus $\mathbb{P}(\alpha_i \leq \rho^{-\frac{1}{2}})$ is in the order of $\rho^{-\frac{1}{2}}$ and $d = \frac{N}{2}$.

Case 3. $L < M$: In this case, the probability of each v_i being negative is nonzero, and thus the probability of α being negative is also nonzero, i.e., $\mathbb{P}(\alpha \leq 0)$ is a constant independent of ρ. Hence, $d = 0$.

B. PROOF OF THEOREM 2

In this subsection, we give the rigorous proof of Theorem 2. The key is to establish lower and upper bounds on the SEP of the following form by applying inequality (12) and characterizing the distribution of α in (13):

$$l_{\text{low}}(\rho)^{-d} + o(\rho^{-d}) \leq \text{SEP} \leq l_{\text{up}}(\rho)^{-d} + o(\rho^{-d}), \tag{18}$$

where $l_{\text{low}}(\rho)$ and $l_{\text{up}}(\rho)$ are linear functions of ρ and $o(\rho^{-d})$ is a high-order infinitesimal of ρ^{-d}, i.e., $o(\rho^{-d})/\rho^{-d} \to 0$. Then we can conclude from the definition in (4) and (18) that the diversity order is d. The most nontrivial steps of the proof is to characterize the distribution of α in (13). Below is the detailed proof of Theorem 2 in three separate cases.

1) PROOF OF THE DIVERSITY ORDER WHEN $L > M$

We first consider the case where $L > M$. To begin, we derive upper and lower bounds on α in (13). Since the quantization error $\theta_i \in [-\frac{\pi}{L}, \frac{\pi}{L}]$, we have

$$\begin{aligned}
\alpha &= \frac{1}{\sqrt{N}} \sum_{i=1}^{N} |h_i| \left(\cos\theta_i - \sin\theta_i \cot\frac{\pi}{M}\right) \\
&\geq \frac{1}{\sqrt{N}} \sum_{i=1}^{N} |h_i| \left(\cos\frac{\pi}{L} - \sin\frac{\pi}{L} \cot\frac{\pi}{M}\right) \\
&= \frac{c_0 \|\mathbf{h}\|_1}{\sqrt{N}} \geq \frac{c_0 \|\mathbf{h}\|_2}{\sqrt{N}},
\end{aligned}$$

where $c_0 = \cos\frac{\pi}{L} - \sin\frac{\pi}{L} \cot\frac{\pi}{M}$ is a positive constant when $L > M$. Similarly, we have $\alpha \leq \frac{\|\mathbf{h}\|_1}{\sqrt{N}} \leq \|\mathbf{h}\|_2$. Using inequality (12) and the above bounds on α, we obtain

$$\text{SEP} \leq 2\mathbb{E}\left[Q\left(\frac{\sqrt{2}\sin\frac{\pi}{M} c_0 \|\mathbf{h}\|_2}{\sqrt{N}\sigma}\right)\right] \tag{19a}$$

and

$$\text{SEP} \geq \mathbb{E}\left[Q\left(\frac{\sqrt{2}\sin\frac{\pi}{M} \|\mathbf{h}\|_2}{\sigma}\right)\right]. \tag{19b}$$

Note that $2\|\mathbf{h}\|_2^2$ is a chi-square random variable with $2N$ degrees of freedom, i.e., $2\|\mathbf{h}\|_2^2 \sim \mathcal{X}^2(2N)$. Hence, the moment generating function of $\|\mathbf{h}\|_2^2$ is

$$\text{MGF}_{\|\mathbf{h}\|_2^2}(t) = \mathbb{E}\left[e^{t\|\mathbf{h}\|_2^2}\right] = (1-t)^{-N}.$$

Applying the well-known inequality $Q(x) \leq \frac{1}{2}e^{-\frac{1}{2}x^2}$, $x \geq 0$ [37] to (19a), we can upper bound the SEP as

$$\begin{aligned} \text{SEP} &\leq \text{MGF}_{\|\mathbf{h}\|_2^2}\left(-\frac{\sin^2\frac{\pi}{M}c_0^2}{N\sigma^2}\right) \\ &= \left(1+\frac{\sin^2\frac{\pi}{M}c_0^2}{N}\rho\right)^{-N}, \end{aligned} \tag{20}$$

where the last equality holds since $\rho = 1/\sigma^2$.

On the other hand, by applying the Craig's representation of the Q-function [39], i.e.,

$$Q(x) = \frac{1}{\pi}\int_0^{\frac{\pi}{2}} e^{-\frac{x^2}{2\sin^2\theta}}d\theta, \quad x \geq 0, \tag{21}$$

to (19b), we can lower bound the SEP as

$$\begin{aligned} \text{SEP} &\geq \mathbb{E}\left[\frac{1}{\pi}\int_0^{\frac{\pi}{2}} e^{-\frac{\sin^2\frac{\pi}{M}\rho\|\mathbf{h}\|_2^2}{\sin^2\theta}}d\theta\right] \\ &= \frac{1}{\pi}\int_0^{\frac{\pi}{2}} \text{MGF}_{\|\mathbf{h}\|_2^2}\left(-\frac{\sin^2\frac{\pi}{M}\rho}{\sin^2\theta}\right)d\theta \\ &= \frac{1}{\pi}\int_0^{\frac{\pi}{2}} \left(1+\frac{\sin^2\frac{\pi}{M}}{\sin^2\theta}\rho\right)^{-N}d\theta, \end{aligned}$$

where the first equality holds since the integrand is nonnegative and thus we are free to change the order of integral and expectation according to the Tonelli-Fubini Theorem (see, e.g., [40]). Similar to [41, Section III-A], we can further obtain the following lower bound on the SEP:

$$\text{SEP} \geq \frac{1}{2\sqrt{\pi(N+\frac{1}{2})}}\left(1+\sin^2\frac{\pi}{M}\rho\right)^{-N}. \tag{22}$$

It follows immediately from (20) and (22) that $d = N$ in this case.

2) PROOF OF THE DIVERSITY ORDER WHEN $L = M$

As discussed in Case 2 in Section IV-A, when $L = M$, both $|h_i|$ and v_i, $i = 1, 2, \ldots, N$, will play roles in the diversity order analysis, in which case the distribution of α needs to be investigated carefully. The following two lemmas give the PDF of α_i and an upper bound on the PDF of α when $L = M$, respectively, which are important for our analysis.

Lemma 1: When $L = M$, the PDF of α_i is given by

$$p_{\alpha_i}(x) = \begin{cases} \frac{2M\sin\frac{\pi}{M}}{\sqrt{\pi}}e^{-\sin^2\frac{\pi}{M}x^2}Q\left(\sqrt{2}\cos\frac{\pi}{M}x\right), & \text{if } x \geq 0; \\ 0, & \text{if } x < 0. \end{cases}$$

Lemma 2: When $L = M$, the PDF of α can be upper bounded as

$$p_\alpha(x) \leq \frac{M^N\sin\frac{\pi}{M}}{\sqrt{\pi}}, \quad x \geq 0.$$

The proofs of Lemmas 1 and 2 are given in Appendix A and B, respectively. Now we are ready to give the diversity order analysis for the case of $L = M$.

We first prove that $d \geq \frac{N}{2}$ by giving an upper bound on the SEP. Note that $\alpha \geq 0$ when $L = M$. Then from (12) and using the fact that $Q(x) \leq \frac{1}{2}e^{-\frac{1}{2}x^2}$ for $x \geq 0$, we have

$$\begin{aligned} \text{SEP} &\leq \mathbb{E}_\alpha\left[e^{-\sin^2\frac{\pi}{M}\rho\alpha^2}\right] \\ &= \int_0^{+\infty} e^{-\sin^2\frac{\pi}{M}\rho x^2}p_\alpha(x)dx. \end{aligned} \tag{23}$$

For any given $\epsilon > 0$, the integral in (23) can be split into the sum of two integrals as

$$\begin{aligned} &\int_0^{+\infty} e^{-\sin^2\frac{\pi}{M}\rho x^2}p_\alpha(x)dx \\ &= \int_0^{\rho^{-\frac{1-\epsilon}{2}}} e^{-\sin^2\frac{\pi}{M}\rho x^2}p_\alpha(x)dx + \int_{\rho^{-\frac{1-\epsilon}{2}}}^{+\infty} e^{-\sin^2\frac{\pi}{M}\rho x^2}p_\alpha(x)dx \\ &\triangleq I_1 + I_2. \end{aligned} \tag{24}$$

Next we give upper bounds on I_1 and I_2 separately. For I_1, recalling the relationship between α and α_i and noting that $e^{-\sin^2\frac{\pi}{M}\rho x^2} \leq 1$, we get the following inequality:

$$\begin{aligned} I_1 &\leq \int_0^{\rho^{-\frac{1-\epsilon}{2}}} p_\alpha(x)dx = \mathbb{P}\left(0 \leq \alpha \leq \rho^{-\frac{1-\epsilon}{2}}\right) \\ &\leq \prod_{i=1}^{N}\mathbb{P}\left(0 \leq \alpha_i \leq \sqrt{N}\rho^{-\frac{1-\epsilon}{2}}\right). \end{aligned} \tag{25}$$

Moreover, it follows from Lemma 1 that

$$\begin{aligned} &\mathbb{P}\left(0 \leq \alpha_i \leq \sqrt{N}\rho^{-\frac{1-\epsilon}{2}}\right) \\ &= \frac{2M\sin\frac{\pi}{M}}{\sqrt{\pi}}\int_0^{\sqrt{N}\rho^{-\frac{1-\epsilon}{2}}} e^{-\sin^2\frac{\pi}{M}x^2}Q\left(\sqrt{2}\cos\frac{\pi}{M}x\right)dx \\ &\leq \frac{M\sqrt{N}\sin\frac{\pi}{M}}{\sqrt{\pi}}\rho^{-\frac{1-\epsilon}{2}}, \end{aligned}$$

where the inequality is due to $e^{-\sin^2\frac{\pi}{M}x^2}Q(\sqrt{2}\cos\frac{\pi}{M}x) \leq \frac{1}{2}$ for $x \geq 0$. Combining the above inequality with (25), we have

$$I_1 \leq \left(\frac{M\sqrt{N}\sin\frac{\pi}{M}}{\sqrt{\pi}}\right)^N \rho^{-\frac{N}{2}(1-\epsilon)}. \tag{26}$$

Now we upper bound I_2 by applying Lemma 2:

$$\begin{aligned} I_2 &\leq \frac{M^N\sin\frac{\pi}{M}}{\sqrt{\pi}}\int_{\rho^{-\frac{1-\epsilon}{2}}}^{+\infty} e^{-\sin^2\frac{\pi}{M}\rho x^2}dx \\ &= \frac{M^N}{\sqrt{\rho}}Q\left(\sqrt{2}\sin\frac{\pi}{M}\rho^{\frac{\epsilon}{2}}\right) \\ &\leq \frac{M^N}{2\sqrt{\rho}}e^{-\sin^2\frac{\pi}{M}\rho^\epsilon}. \end{aligned} \tag{27}$$

It follows from (23)–(27) that

$$\text{SEP} \leq \left(\frac{M\sqrt{N}\sin\frac{\pi}{M}}{\sqrt{\pi}}\right)^N \rho^{-\frac{N}{2}(1-\epsilon)} + \frac{M^N}{2\sqrt{\rho}} e^{-\sin^2\frac{\pi}{M}\rho^{\epsilon}},$$

which implies that $d \geq \frac{N}{2}(1-\epsilon)$. Since the above inequality holds for any $\epsilon > 0$, we have $d \geq \frac{N}{2}$.

Next we give a lower bound on the SEP, which in turn gives an upper bound on d. Applying inequality (12) and the Craig's representation of the Q-function in (21), we have

$$\text{SEP} \geq \frac{1}{\pi}\int_0^{\frac{\pi}{2}}\int_0^{+\infty} e^{-\frac{\sin^2\frac{\pi}{M}\rho x^2}{\sin^2\theta}} p_\alpha(x)dxd\theta, \tag{28}$$

where we have changed the order of integral according to the Tonelli-Fubini Theorem. Focusing on the inner integral, we have

$$\begin{aligned}\int_0^{+\infty} e^{-\frac{\sin^2\frac{\pi}{M}\rho x^2}{\sin^2\theta}} p_\alpha(x)dx &\geq \int_0^{\rho^{-\frac{1}{2}}} e^{-\frac{\sin^2\frac{\pi}{M}\rho x^2}{\sin^2\theta}} p_\alpha(x)dx \\ &\geq \mathbb{P}\left(0 \leq \alpha \leq \rho^{-\frac{1}{2}}\right) e^{-\frac{\sin^2\frac{\pi}{M}}{\sin^2\theta}},\end{aligned}$$

which, together with (21) and (28), further implies

$$\text{SEP} \geq Q\left(\sqrt{2}\sin\frac{\pi}{M}\right)\mathbb{P}\left(0 \leq \alpha \leq \rho^{-\frac{1}{2}}\right). \tag{29}$$

The term $\mathbb{P}(0 \leq \alpha \leq \rho^{-\frac{1}{2}})$ in (29) can further be lower bounded as

$$\mathbb{P}\left(0 \leq \alpha \leq \rho^{-\frac{1}{2}}\right) \geq \prod_{i=1}^{N}\mathbb{P}\left(0 \leq \alpha_i \leq \frac{\rho^{-\frac{1}{2}}}{\sqrt{N}}\right). \tag{30}$$

According to Lemma 1,

$$\begin{aligned}&\mathbb{P}\left(0 \leq \alpha_i \leq \frac{\rho^{-\frac{1}{2}}}{\sqrt{N}}\right) \\ &= \frac{2M\sin\frac{\pi}{M}}{\sqrt{\pi}}\int_0^{(N\rho)^{-\frac{1}{2}}} e^{-\sin^2\frac{\pi}{M}x^2} Q\left(\sqrt{2}\cos\frac{\pi}{M}x\right)dx.\end{aligned}$$

When ρ is sufficiently large, we have

$$e^{-\sin^2\frac{\pi}{M}x^2} Q\left(\sqrt{2}\cos\frac{\pi}{M}x\right) \geq \frac{1}{4}, x \in \left[0, (N\rho)^{-\frac{1}{2}}\right],$$

and thus

$$\mathbb{P}\left(0 \leq \alpha_i \leq \frac{\rho^{-\frac{1}{2}}}{\sqrt{N}}\right) \geq \frac{M\sin\frac{\pi}{M}\rho^{-\frac{1}{2}}}{2\sqrt{N\pi}}. \tag{31}$$

Combining (29)–(31) yields the following lower bound on the SEP:

$$\text{SEP} \geq Q\left(\sqrt{2}\sin\frac{\pi}{M}\right)\left(\frac{M\sin\frac{\pi}{M}\rho^{-\frac{1}{2}}}{2\sqrt{N\pi}}\right)^N,$$

which further implies $d \leq \frac{N}{2}$. In conclusion, we have $d = \frac{N}{2}$.

3) PROOF OF THE DIVERSITY ORDER WHEN $L < M$

Finally, we prove that $d = 0$ when $L < M$. Using inequality (12) and the fact that $Q(x) \geq \frac{1}{2}$ for $x \leq 0$, we have

$$\begin{aligned}\text{SEP} &\geq \mathbb{E}_\alpha\left[Q\left(\frac{\sqrt{2}\sin\frac{\pi}{M}\alpha}{\sigma}\right)\right] \\ &\geq \frac{1}{2}\mathbb{P}(\alpha \leq 0) \geq \frac{1}{2}\prod_{i=1}^{N}\mathbb{P}(\alpha_i \leq 0) \\ &= \frac{1}{2}\prod_{i=1}^{N}\mathbb{P}(v_i \leq 0),\end{aligned} \tag{32}$$

where the last equality holds since $\alpha_i = |h_i|v_i$ (see (16)) and $|h_i| \geq 0$. Using similar arguments as in Lemma 3 in Appendix A, we can derive the CDF of v_i for $L < M$:

$$F_{v_i}(x) = 1 - \frac{L}{M} + \frac{L\arcsin\left(x\sin\frac{\pi}{M}\right)}{\pi}, \text{ if } L < M,$$

and hence

$$\mathbb{P}(v_i \leq 0) = F_{v_i}(0) = 1 - \frac{L}{M} > 0. \tag{33}$$

Substituting the above inequality into (32) gives

$$\text{SEP} \geq \frac{1}{2}\left(1 - \frac{L}{M}\right)^N,$$

which, together with the definition in (4), shows

$$0 \leq d \leq \lim_{\rho\to\infty}\frac{-\ln\frac{1}{2}(1-L/M)^N}{\ln\rho} = 0,$$

i.e., $d = 0$.

We remark here that (33) holds regardless of the channel distribution, and hence the above diversity order result for $L < M$ (i.e., $d = 0$) holds for any generic channel.

V. NUMERICAL RESULTS

In this section, we provide simulation results to verify the diversity order results in Theorem 2. All results are averaged over 10^9 channel realizations.

In Figs. 2 and 3, we consider QPSK constellation with $N = 2$ and 8-PSK constellation with $N = 4$, respectively. We depict the SER as a function of the SNR and consider different numbers of quantization levels, i.e., $L = M-1$, $L = M$, $L = M+1$, and $L = \infty$, to demonstrate the effect of the number of quantization levels on the diversity order. For clarity, we also report the lines with slopes $-N$ and $-\frac{N}{2}$ to compare the simulation results with the analytical results. As shown in the figures, the curve of $L = M+1$ is parallel to the curve of $L = \infty$ in the high SNR regime, both of which are parallel to the line with slope $-N$; when $L = M$, the slope of the SER curve is nearly $-\frac{N}{2}$ when the SNR is high; and when $L < M$, there is an SER floor at high SNRs, i.e., the slope of the SER curve is 0. These observations are consistent with the diversity order results in Theorem 2.

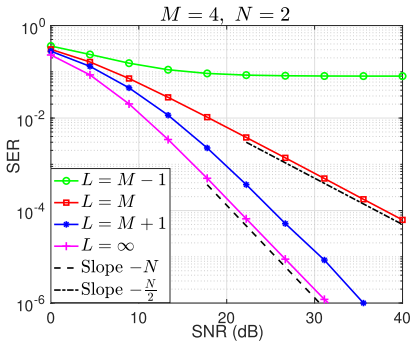

FIGURE 2. The SER versus the SNR, for different numbers of quantization levels L with $M = 4$ and $N = 2$.

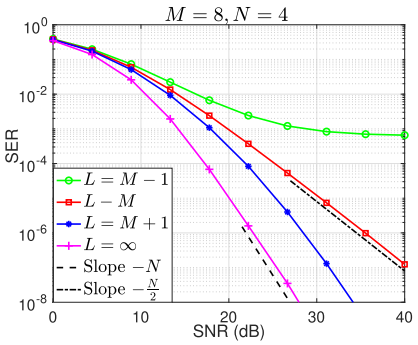

FIGURE 3. The SER versus the SNR, for different numbers of quantization levels of L with $M = 8$ and $N = 4$.

VI. CONCLUSION

This paper characterized the diversity order of QCE transmission for a downlink single-user MISO system with M-PSK modulation. It has been shown that for the L-level quantized MF precoder, full diversity order is achievable when $L > M$, while only half and zero diversity order can be achieved when $L = M$ and $L < M$, respectively. Simulation results verified our diversity order results.

An important and interesting future work is to analyze the SEP performance of the multi-user QCE system. By simulations, we have observed that as the SNR grows, the SEP of the multi-user system does not decrease to zero and there is a positive SEP floor even when the number of quantization levels is infinite, which is in sharp contrast to the single-user case. Therefore, the diversity order considered in this paper is no longer an appropriate performance metric in the multi-user scenario. Instead, it would be interesting to characterize the SEP floor at the infinite SNR for different numbers of quantization levels. The SEP analysis of the multi-user system requires more sophisticated tools due to the more complicated system model.

APPENDIX A
PROOF OF LEMMA 1

Our goal in this section is to calculate the PDF of $\alpha_i = |h_i|v_i$ in (16) for the case where $L = M$. Note that $2|h_i|^2 \sim \mathcal{X}^2(2)$. Then the PDF of $|h_i|$ is given by $p_{|h_i|}(x) = 2xe^{-x^2}, x \geq 0$. We next calculate the PDF of v_i.

Lemma 3: When $L = M$, the PDF of v_i is given by

$$p_{v_i}(x) = \begin{cases} \frac{M \sin \frac{\pi}{M}}{\pi \sqrt{1-\sin^2 \frac{\pi}{M} x^2}}, & \text{if } x \in [0,1]; \\ 0, & \text{otherwise.} \end{cases}$$

Proof: From the definition of v_i in (16), we have

$$\begin{aligned} v_i &= \cos\theta_i - |\sin\theta_i| \cot\frac{\pi}{M} \\ &= \cos|\theta_i| - \sin|\theta_i| \cot\frac{\pi}{M} \\ &= \frac{\sin\left(\frac{\pi}{M} - |\theta_i|\right)}{\sin\frac{\pi}{M}}, \end{aligned} \tag{34}$$

where $|\theta_i|$ is uniformly distributed in $[0, \frac{\pi}{M}]$ and the second equality holds since $|\theta_i| \leq \frac{\pi}{M} \leq \frac{\pi}{2}$. It follows immediately that $0 \leq v_i \leq 1$. Therefore, if $x \notin [0,1]$, $p_{v_i}(x) = 0$; if $x \in [0,1]$, the CDF of v_i is

$$\begin{aligned} F_{v_i}(x) &= \mathbb{P}(v_i \leq x) \\ &= \mathbb{P}\left(|\theta_i| \geq \frac{\pi}{M} - \arcsin\left(x \sin\frac{\pi}{M}\right)\right) \\ &= \frac{M \arcsin\left(x \sin\frac{\pi}{M}\right)}{\pi}. \end{aligned} \tag{35}$$

Taking the derivative with respect to x on both sides of (35) gives the desired result. ■

The following lemma gives the PDF of the product of two independent random variables.

Lemma 4 ([42, p135]): Let X and Y be two independent random variables with PDFs $p_X(\cdot)$ and $p_Y(\cdot)$. Then the PDF of $Z = XY$ is

$$p_Z(z) = \int_{-\infty}^{+\infty} \frac{1}{|x|} p_X(x) p_Y\left(\frac{z}{x}\right) dx.$$

With the above two lemmas, we are now ready to compute the PDF of α_i. Applying Lemma 4 to $\alpha_i = v_i|h_i|$, we have

$$p_{\alpha_i}(x) = \begin{cases} \int_0^1 \frac{1}{z} p_{v_i}(z) p_{|h_i|}\left(\frac{x}{z}\right) dz, & \text{if } x \geq 0; \\ 0, & \text{if } x < 0. \end{cases}$$

Now we simplify the above PDF expression for $x \geq 0$:

$$\begin{aligned} p_{\alpha_i}(x) &= \frac{2M \sin\frac{\pi}{M}}{\pi} \int_0^1 \frac{x}{z^2 \sqrt{1 - \sin^2\frac{\pi}{M} z^2}} e^{-\frac{x^2}{z^2}} dz \\ &\overset{z=\frac{\sin\theta}{\sin\frac{\pi}{M}}}{=\!=\!=} \frac{2M \sin^2\frac{\pi}{M}}{\pi} \int_0^{\frac{\pi}{M}} \frac{x}{\sin^2\theta} e^{-\frac{\sin^2\frac{\pi}{M} x^2}{\sin^2\theta}} d\theta. \end{aligned} \tag{36}$$

Letting $u = \sin\frac{\pi}{M} x \cot\theta$, then

$$\begin{aligned} &\int_0^{\frac{\pi}{M}} \frac{x}{\sin^2\theta} e^{-\frac{\sin^2\frac{\pi}{M} x^2}{\sin^2\theta}} d\theta \\ &= \frac{1}{\sin\frac{\pi}{M}} e^{-\sin^2\frac{\pi}{M} x^2} \int_{\cos\frac{\pi}{M} x}^{+\infty} e^{-u^2} du \end{aligned}$$

$$= \frac{\sqrt{\pi} e^{-\sin^2 \frac{\pi}{M} x^2}}{\sin \frac{\pi}{M}} Q\left(\sqrt{2} \cos \frac{\pi}{M} x\right).$$

Combining the above equality with (36) gives the PDF of α_i for $x \geq 0$ and completes the proof.

APPENDIX B
PROOF OF LEMMA 2

In this section, we prove Lemma 2. Let $S_n = \sum_{i=1}^{n} \alpha_i$, $n = 1, 2, \ldots, N$. Then $\alpha = \frac{S_N}{\sqrt{N}}$. According to Lemma 1, the PDF of each α_i is zero when $x < 0$, and thus $p_\alpha(x)$ is zero when $x < 0$. When $x \geq 0$, we claim that the following inequality holds:

$$p_{S_n}(x) \leq \frac{M^n \sin \frac{\pi}{M}}{\sqrt{n\pi}} e^{-\frac{1}{n} \sin^2 \frac{\pi}{M} x^2}, x \geq 0, \tag{37}$$

which further implies that

$$p_\alpha(x) = \sqrt{N} p_{S_N}(\sqrt{N}x) \leq \frac{M^N \sin \frac{\pi}{M}}{\sqrt{\pi}}, x \geq 0.$$

We next prove (37) by induction. Note that $Q(x) \leq \frac{1}{2}$ for all $x \geq 0$, and thus the inequality holds immediately for $n = 1$. Now suppose that (37) holds for some n with $1 < n < N$. Then for S_{n+1}, we have

$$\begin{aligned}
&p_{S_{n+1}}(x) \\
&= \int_{-\infty}^{+\infty} p_{S_n}(y) p_{\alpha_{n+1}}(x-y) dy \\
&\leq \int_0^x \frac{M^n \sin \frac{\pi}{M}}{\sqrt{n\pi}} e^{-\frac{1}{n} \sin^2 \frac{\pi}{M} y^2} \frac{M \sin \frac{\pi}{M}}{\sqrt{\pi}} e^{-\sin^2 \frac{\pi}{M} (x-y)^2} dy \\
&\leq \frac{M^{n+1} \sin^2 \frac{\pi}{M}}{\sqrt{n\pi}} \int_{-\infty}^{+\infty} e^{-\frac{1}{n} \sin^2 \frac{\pi}{M} y^2} e^{-\sin^2 \frac{\pi}{M} (x-y)^2} dy \\
&= \frac{M^{n+1} \sin \frac{\pi}{M}}{\sqrt{(n+1)\pi}} e^{-\frac{1}{n+1} \sin^2 \frac{\pi}{M} x^2},
\end{aligned}$$

where the first inequality uses (37) for n and Lemma 1 and the second inequality is due to the change of the integral interval. The above inequality shows that (37) holds for $n+1$ and completes the proof.

REFERENCES

[1] F. Rusek et al., "Scaling up MIMO: Opportunities and challenges with very large arrays," *IEEE Signal Process. Mag.*, vol. 30, no. 1, pp. 40–60, Jan. 2013.

[2] J. G. Andrews et al., "What will 5G be?," *IEEE J. Sel. Areas Commun.*, vol. 32, no. 6, pp. 1065–1082, Jun. 2014.

[3] L. Lu, G. Y. Li, A. L. Swindlehurst, A. Ashikhmin, and R. Zhang, "An overview of massive MIMO: Benefits and challenges," *IEEE J. Sel. Topics Signal Process.*, vol. 8, no. 5, pp. 742–758, Oct. 2014.

[4] O. Blume, D. Zeller, and U. Barth, "Approaches to energy efficient wireless access networks," in *Proc. IEEE 4th Int. Symp. Commun. Control Signal Process.*, 2010, pp. 1–5.

[5] S. K. Mohammed and E. G. Larsson, "Single-user beamforming in large-scale MISO systems with per-antenna constant-envelope constraints: The doughnut channel," *IEEE Trans. Wireless Commun.*, vol. 11, no. 11, pp. 3992–4005, Nov. 2012.

[6] S. K. Mohammed and E. G. Larsson, "Per-antenna constant envelope precoding for large multi-user MIMO systems," *IEEE Trans. Commun.*, vol. 61, no. 2, pp. 1059–1071, Mar. 2013.

[7] J. Pan and W.-K. Ma, "Constant envelope precoding for single-user large-scale MISO channels: Efficient precoding and optimal designs," *IEEE J. Sel. Topics Signal Process.*, vol. 8, no. 5, pp. 982–995, Oct. 2014.

[8] J. Zhang, Y. Huang, J. Wang, B. Ottersten, and L. Yang, "Per-antenna constant envelope precoding and antenna subset selection: A geometric approach," *IEEE Trans. Signal Process.*, vol. 64, no. 23, pp. 6089–6104, Dec. 2016.

[9] P. V. Amadori and C. Masouros, "Constant envelope precoding by interference exploitation in phase shift keying-modulated multiuser transmission," *IEEE Trans. Wireless Commun.*, vol. 16, no. 1, pp. 538–550, Jan. 2017.

[10] F. Liu, C. Masouros, P. V. Amadori, and H. Sun, "An efficient manifold algorithm for constructive interference based constant envelope precoding," *IEEE Signal Process. Lett.*, vol. 24, no. 10, pp. 1542–1546, Oct. 2017.

[11] S. Zhang, R. Zhang, and T. J. Lim, "Constant envelope precoding for MIMO systems," *IEEE Trans. Commun.*, vol. 66, no. 1, pp. 149–162, Jan. 2018.

[12] Z. Wei, C. Masouros, and F. Liu, "Secure directional modulation with few-bit phase shifters: Optimal and iterative-closed-form designs," *IEEE Trans. Commun.*, vol. 69, no. 1, pp. 486–500, Jan. 2021.

[13] S. Ahmed, J. S. Thompson, Y. R. Petillot, and B. Mulgrew, "Finite alphabet constant-envelope waveform design for MIMO radar," *IEEE Trans. Signal Process.*, vol. 59, no. 11, pp. 5326–5337, Nov. 2011.

[14] H. Yang, X. Yuan, J. Fang, and Y.-C. Liang, "Reconfigurable intelligent surface aided constant-envelope wireless power transfer," *IEEE Trans. Signal Process.*, vol. 69, pp. 1347–1361, Feb. 2021.

[15] R. Walden, "Analog-to-digital converter survey and analysis," *IEEE J. Sel. Areas Commun.*, vol. 17, no. 4, pp. 539–550, Apr. 1999.

[16] M. Kazemi, H. Aghaeinia, and T. M. Duman, "Discrete-phase constant envelope precoding for massive MIMO systems," *IEEE Trans. Commun.*, vol. 65, no. 5, pp. 2011–2021, May 2017.

[17] H. Jedda, A. Mezghani, A. L. Swindlehurst, and J. A. Nossek, "Quantized constant envelope precoding with PSK and QAM signaling," *IEEE Trans. Wireless Commun.*, vol. 17, no. 12, pp. 8022–8034, Dec. 2018.

[18] J.-C. Chen, "Efficient constant envelope precoding with quantized phases for massive MU-MIMO downlink systems," *IEEE Trans. Veh. Technol.*, vol. 68, no. 4, pp. 4059–4063, Apr. 2019.

[19] M. Shao, Q. Li, W.-K. Ma, and A. M. -C. So, "A framework for one-bit and constant-envelope precoding over multiuser massive MISO channels," *IEEE Trans. Signal Process.*, vol. 67, no. 20, pp. 5309–5324, Oct. 2019.

[20] C.-J. Wang, C.-K. Wen, S. Jin, and S.-H. Tsai, "Finite-alphabet precoding for massive MU-MIMO with low-resolution DACs," *IEEE Trans. Wireless Commun.*, vol. 17, no. 7, pp. 4706–4720, Jul. 2018.

[21] S. Jacobsson, G. Durisi, M. Coldrey, T. Goldstein, and C. Studer, "Quantized precoding for massive MU-MIMO," *IEEE Trans. Commun.*, vol. 65, no. 11, pp. 4670–4684, Nov. 2017.

[22] O. Castañeda, S. Jacobsson, G. Durisi, M. Coldrey, T. Goldstein, and C. Studer, "1-bit massive MU-MIMO precoding in VLSI," *IEEE J. Emerg. Sel. Topics Circuits Syst.*, vol. 7, no. 4, pp. 508–522, Dec. 2017.

[23] F. Sohrabi, Y.-F. Liu, and W. Yu, "One-bit precoding and constellation range design for massive MIMO with QAM signaling," *IEEE J. Sel. Topics Signal Process.*, vol. 12, no. 3, pp. 557–570, Jun. 2018.

[24] H. Jedda, A. Mezghani, J. A. Nossek, and A. L. Swindlehurst, "Massive MIMO downlink 1-bit precoding with linear programming for PSK signaling," in *Proc. IEEE Workshop Signal Process. Adv. Wireless Commun.*, 2017, pp. 1–5.

[25] A. Li, C. Masouros, F. Liu, and A. L. Swindlehurst, "Massive MIMO 1-bit DAC transmission: A low-complexity symbol scaling approach," *IEEE Trans. Wireless Commun.*, vol. 17, no. 11, pp. 7559–7575, Nov. 2018.

[26] A. Li, F. Liu, C. Masouros, Y. Li, and B. Vucetic, "Interference exploitation 1-bit massive MIMO precoding: A partial branch-and-bound solution with near-optimal performance," *IEEE Trans. Wireless Commun.*, vol. 19, no. 5, pp. 3474–3489, May 2020.

[27] Z. Wu, B. Jiang, Y.-F. Liu, and Y.-H. Dai, "A novel negative ℓ_1 penalty approach for multiuser one-bit massive MIMO downlink with PSK signaling," in *Proc. IEEE Int. Conf. Acoust., Speech, Signal Process.*, 2022, pp. 5323–5327.

[28] Z. Wu, B. Jiang, Y.-F. Liu, and Y.-H. Dai, "CI-based one-bit precoding for multiuser downlink massive MIMO systems with PSK modulation: A negative ℓ_1 penalty approach," 2021. [Online]. Available: https://arxiv.org/abs/2110.11628
[29] Y. Li, C. Tao, A. Lee Swindlehurst, A. Mezghani, and L. Liu, "Downlink achievable rate analysis in massive MIMO systems with one-bit DACs," *IEEE Commun. Lett.*, vol. 21, no. 7, pp. 1669–1672, Jul. 2017.
[30] S. Jacobsson, G. Durisi, M. Coldrey, and C. Studer, "Linear precoding with low-resolution DACs for massive MU-MIMO-OFDM downlink," *IEEE Trans. Wireless Commun.*, vol. 18, no. 3, pp. 1595–1609, Mar. 2019.
[31] A. K. Saxena, I. Fijalkow, and A. L. Swindlehurst, "Analysis of one-bit quantized precoding for the multiuser massive MIMO downlink," *IEEE Trans. Signal Process.*, vol. 65, no. 17, pp. 4624–4634, Sep. 2017.
[32] C. Masouros, T. Ratnarajah, M. Sellathurai, C. B. Papadias, and A. K. Shukla, "Known interference in the cellular downlink: A performance limiting factor or a source of green signal power?," *IEEE Commun. Mag.*, vol. 51, no. 10, pp. 162–171, Oct. 2013.
[33] C. Masouros, M. Sellathurai, and T. Ratnarajah, "Vector perturbation based on symbol scaling for limited feedback MISO downlinks," *IEEE Trans. Signal Process.*, vol. 62, no. 3, pp. 562–571, Feb. 2014.
[34] A. Li et al., "A tutorial on interference exploitation via symbol-level precoding: Overview, state-of-the-art and future directions," *IEEE Commun. Surveys Tuts.*, vol. 22, no. 2, pp. 796–839, Apr.–Jun. 2020.
[35] L. Zheng and D. Tse, "Diversity and multiplexing: A fundamental tradeoff in multiple-antenna channels," *IEEE Trans. Inf. Theory*, vol. 49, no. 5, pp. 1073–1096, May 2003.
[36] M. Shao, Q. Li, Y. Liu, and W.-K. Ma, "Multiuser one-bit massive MIMO precoding under MPSK signaling," in *Proc. IEEE Glob. Conf. Signal Inf. Process*., 2018, pp. 833–837.
[37] J. G. Proakis and M. Salehi, *Digital Communications*, 5th ed. New York, NY, USA: McGraw-Hill, 2008.
[38] S. Gayan, R. Senanayake, H. Inaltekin, and J. Evans, "Low-resolution quantization in phase modulated systems: Optimum detectors and error rate analysis," *IEEE Open J. Commun. Soc.*, vol. 1, pp. 1000–1021, 2020.
[39] J. Craig, "A new, simple, and exact result for calculating the probability of error for two-dimensional signal constellations," in *Proc. IEEE Mil. Commun. Conf.*, 1991, pp. 571–575.
[40] R. M. Dudley, *Real Analysis and Probability*, 2nd ed. Cambridge, U.K.: Cambridge Univ. Press, 2002.
[41] R. Jiang and Y.-F. Liu, "Antenna efficiency in massive MIMO detection," in *Proc. IEEE Workshop Signal Process. Adv. Wireless Commun.*, 2021, pp. 51–55.
[42] V. Rohatgi and A. Saleh, *An Introduction to Probability and Statistics*, 3rd ed. Hoboken, NJ, USA: Wiley, 2015.

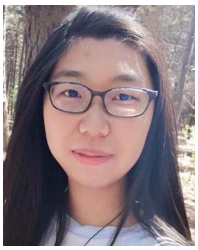

ZHEYU WU (Graduate Student Member, IEEE) received the B.Sc. degree in applied mathematics from Jilin University, Changchun, China, in 2019. She is currently working toward the Ph.D. degree with the Institute of Computational Mathematics and Scientific/Engineering Computing, Academy of Mathematics and Systems Science, Chinese Academy of Sciences, Beijing, China. Her main research interests include optimization algorithm and its applications to signal processing and wireless communications.

JIAGENG WU received the M.Sc. degree in computer science from Brandeis University, Waltham, MA, USA, in 2020. He is currently working toward the Ph.D. degree with the Jilin University, Changchun, China. His main research interests include optimization algorithm and its applications to signal processing and wireless communications.

WEI-KUN CHEN received the B.Sc. degree in information and computing science from Sun Yat-Sen University, Guangzhou, China, in 2014, and the Ph.D. degree in computational mathematics from the Chinese Academy of Sciences, Beijing, China, in 2019. In 2019, he joined the School of Mathematics and Statistics, Beijing Institute of Technology, Beijing, China, where he is currently an Assistant Professor. His main research interests include mixed integer programming and its applications to wireless communications.

YA-FENG LIU (Senior Member, IEEE) received the B.Sc. degree in applied mathematics from Xidian University, Xi'an, China, in 2007, and the Ph.D. degree in computational mathematics from the Chinese Academy of Sciences (CAS), Beijing, China, in 2012. From 2011 to 2012, he was supported by the Academy of Mathematics and Systems Science (AMSS), CAS, to visit Professor Zhi-Quan (Tom) Luo with the University of Minnesota (Twins Cities), Minneapolis, MN, USA, during the Ph.D. degree. In 2012, after the Graduation, he joined the Institute of Computational Mathematics and Scientific/Engineering Computing, AMSS, CAS, where he became an Associate Professor in 2018. His main research interests include nonlinear optimization and its applications to signal processing, wireless communications, and machine learning.

Dr. Liu is currently an Associate Editor for the IEEE TRANSACTIONS ON SIGNAL PROCESSING, IEEE SIGNAL PROCESSING LETTERS, and *Journal of Global Optimization*. From 2019 to 2022, he was the Editor of the IEEE TRANSACTIONS ON WIRELESS COMMUNICATIONS. He is also an Elected Member of the Signal Processing for Communications and Networking Technical Committee (SPCOM-TC) of the IEEE Signal Processing Society from 2020–2022 and from 2023–2025. He was the recipient of the Best Paper Award from the IEEE International Conference on Communications (ICC) in 2011, the Chen Jingrun Star Award from the AMSS in 2018, the Science and Technology Award for Young Scholars from the Operations Research Society of China in 2018, the 15th IEEE ComSoc Asia-Pacific Outstanding Young Researcher Award in 2020, and the Science and Technology Award for Young Scholars from China Society for Industrial and Applied Mathematics in 2022. Students supervised and co-supervised by him won the Best Student Paper Award from the International Symposium on Modeling and Optimization in Mobile, Ad Hoc and Wireless Networks (WiOpt) in 2015 and the Best Student Paper Award of IEEE International Conference on Acoustics, Speech and Signal Processing (ICASSP) in 2022.